J. Fluid Mech. (2003), *vol.* 479, *pp.* 221–230.
DOI: 10.1017/S0022112003003756 Printed in the United Kingdom

Schmidt number dependence of derivative moments for quasi-static straining motion

By J. SCHUMACHER[1], K. R. SREENIVASAN[2] AND P. K. YEUNG[3]

[1]Fachbereich Physik, Philipps-Universität, D-35032 Marburg, Germany

[2]Institute for Physical Science and Technology, University of Maryland, College Park, MD 20742, USA

[3]School of Aerospace Engineering, Georgia Institute of Technology, Atlanta, GA 30332, USA

(Received 30 September 2002 and in revised form 2 January 2003)

Bounds on high-order derivative moments of a passive scalar are obtained for large values of the Schmidt number, Sc. The procedure is based on the approach pioneered by Batchelor for the viscous–convective range. The upper bounds for derivative moments of order n are shown to grow as $Sc^{n/2}$ for very large Schmidt numbers. The results are consistent with direct numerical simulations of a passive scalar, with Sc from 1/4 to 64, mixed by homogeneous isotropic turbulence. Although the analysis does not provide proper bounds for normalized moments, the combination of analysis and numerical data suggests that they decay with Sc, at least for odd orders.

1. Introduction

We are interested in understanding the dependence of the statistical properties of a passive scalar on its Schmidt number, Sc, this being the ratio of kinematic viscosity ν of the fluid to the diffusivity κ of the scalar. In some cases, the temperature field of the flow is considered a passive scalar with an equivalently defined Prandtl number, Pr. Obukhov (1949), Yaglom (1949), Corrsin (1951), Batchelor (1959), Kraichnan (1968), and others, have considered specific instances in which Sc assumed different values and limits, but detailed investigations of the Sc-dependence are rare. Experimentally, large values of Sc are obtained when various dyes are mixed in water, and the requirements on instrument resolution (e.g. Prasad & Sreenivasan 1990; Dahm, Southerland & Buch 1991; Saylor & Sreenivasan 1998) are quite severe. For the same reason, three-dimensional direct numerical simulations (DNS) require fine grid resolutions when Sc is large (see Bogucki, Domaradzki & Yeung 1997; Antonia & Orlandi 2002; Yeung, Xu & Sreenivasan 2002; Brethouwer, Hunt & Nieuwstadt 2003).

Of particular interest is the likelihood that the anisotropy of passive scalars driven by a mean scalar gradient persists at high Reynolds numbers, contrary to the premise of local isotropy. This can be seen by plotting the normalized derivative moments

$$S_n(\partial\theta/\partial x) = \frac{\langle(\partial\theta/\partial x)^n\rangle}{\langle(\partial\theta/\partial x)^2\rangle^{n/2}}, \tag{1.1}$$

where x is the direction of the mean scalar gradient, against the Taylor microscale Reynolds number, R_λ. Even the skewness, which corresponds to the lowest-order non-trivial case, does not show a decreasing trend with respect to R_λ for R_λ up to 10^4 (see, for example, figure 7 of Sreenivasan & Antonia 1997). Note that local isotropy (which requires the skewness to vanish) is a prerequisite for the classical

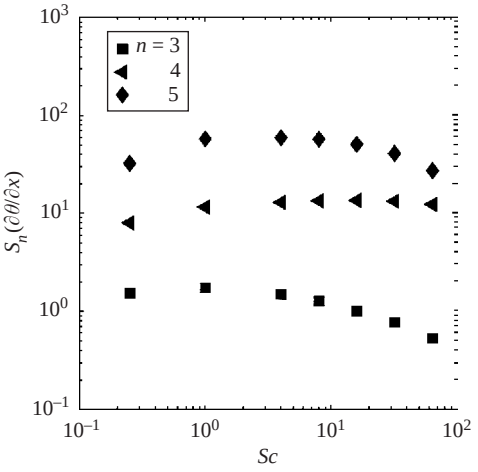

FIGURE 1. Normalized scalar derivative moments for $n = 3, 4$ and 5 (cf. equation (1.1)) as functions of the Schmidt number Sc. The underlying turbulent flow field had a Taylor–Reynolds number $R_\lambda = 38$. The odd normalized moments decrease with Sc but the fourth moment changes little. Data are from Yeung *et al.* (2002).

phenomenology of passive scalars to be valid (Obukhov 1949; Yaglom 1949; Corrsin 1951). It is well-known from measurements (e.g. Gibson, Friehe & McConnell 1977; Sreenivasan, Antonia & Britz 1979) and DNS (Holzer & Siggia 1994; Pumir 1994; Celani *et al.* 2001) that passive scalars develop a ramp–cliff structure when driven by a mean gradient. These structures are thought to make persistent contributions to odd moments of derivatives. As Sc increases, the mixing of the scalar proceeds to increasingly smaller scales beyond the dissipative scale and develops increasingly steeper gradients. However, it is not obvious that these steeper gradients, being further removed from the large scale, will retain a directional preference on the average. This leads us to ask whether, with increasing Sc, there exists a compensation for the directional anisotropy of the large scales, and a consequent diminution of the skewness.

This possibility is supported by recent high-Sc DNS of Yeung *et al.* (2002) on a 512^3 grid. The passive scalar was advected by three-dimensional homogeneous and isotropic turbulence for $1/4 \leqslant Sc \leqslant 64$. The required resolution was achieved by keeping R_λ at a small value of 38. The passive scalar was driven by a constant mean gradient G in one direction. Figure 1 shows the normalized derivative moments S_n of $\partial\theta/\partial x$, for orders three, four and five. While the fourth moment hardly changes with Sc, odd moments do show decreasing trends. It would be of interest to know the asymptotic behaviour for very large Sc and for moments of all orders, although this issue can be resolved only for relatively low Reynolds numbers. It was thus thought that a theoretical analysis, even if incomplete in some respects, might be useful. This is the goal of this paper.

The basis for analysing scalar mixing for high Sc is provided by two classical approaches. Batchelor (1959) discussed scalar advection in the smooth and slowly varying velocity field of small-scale turbulence. This work led to the prediction of a k^{-1} power law for the scalar spectral density in the viscous–convective range (i.e. the range between the Kolmogorov scale $\eta = (\nu^3/\epsilon)^{1/4}$, around which viscous effects become important, and the Batchelor scale $\eta_B = Sc^{-1/2}\eta$, around which the diffusive

effects of the scalar become important). Kraichnan (1968) showed that the k^{-1} scaling obtains even if the spatially smooth velocity field varies rapidly in time. Kraichnan's velocity field is uncorrelated in time and has an infinitesimally small viscous time scale, i.e. the Kolmogorov time scale $\tau_\eta \equiv (\nu/\epsilon)^{1/2} \to 0$. Thus the model operates in the limit $Sc \to 0$ (although the Péclet number can be large), and is therefore unrelated to the present work, whose central concern is the effect of Sc when it is large. A few comments are, however, in order. In a recent work, E & Vanden-Eijnden (2001) provide a consistent re-definition of Sc for scalar advection in such flows. Secondly, using the large deviation theory of Balkovsky & Fouxon (1999), they generalize Kraichnan's work within the Lagrangian picture of scalar advection. When the correlation time of the rates of strain is finite but small compared to an outer scale, they discuss a general form of the probability density function of the scalar and its gradients, and conclude that, because the gradient statistics are non-universal, further progress requires the specification of statistics of the fluctuating strain rates. The quasi-stationarity of the strain field in the Batchelor model removes this impediment, and so it is applied here to discuss the Sc-dependence of scalar derivative moments in the presence of a mean scalar gradient, especially for $Sc > 1$.

2. Balance equations for derivative moments in smooth velocity fields

The (total) scalar field, $\Theta(\boldsymbol{x}, t)$ is composed of a turbulent part, $\theta(\boldsymbol{x}, t)$, and a linear mean part with a constant scalar gradient vector, $\boldsymbol{G}$,

$$\Theta(\boldsymbol{x}, t) = \theta(\boldsymbol{x}, t) + \nabla\langle\Theta\rangle(\boldsymbol{x}) \cdot \boldsymbol{x} \equiv \theta(\boldsymbol{x}, t) - \boldsymbol{G} \cdot \boldsymbol{x}. \tag{2.1}$$

Such a mean scalar gradient can be externally prescribed, e.g. by selective heating of wind-tunnel walls or by adjusting the resistance distribution at the wind-tunnel inlet. The advection–diffusion equation for $\Theta(\boldsymbol{x}, t)$ has the form

$$\partial_t \Theta(\boldsymbol{x}, t) + \boldsymbol{u}(\boldsymbol{x}, t) \cdot \nabla\Theta(\boldsymbol{x}, t) = \kappa\nabla^2\Theta(\boldsymbol{x}, t). \tag{2.2}$$

When (2.1) is inserted in (2.2), we obtain, for the turbulent part,

$$\partial_t \theta(\boldsymbol{x}, t) + \boldsymbol{u}(\boldsymbol{x}, t) \cdot \nabla\theta(\boldsymbol{x}, t) = \kappa\nabla^2\theta(\boldsymbol{x}, t) + \boldsymbol{u}(\boldsymbol{x}, t) \cdot \boldsymbol{G}. \tag{2.3}$$

The quantity $\boldsymbol{u} \cdot \boldsymbol{G}$ is a production term which ensures statistical stationarity of $\theta(\boldsymbol{x}, t)$. After taking the partial derivative with respect to the coordinate i, which may be x, y or z, and multiplying by $(\partial_i\theta)^{n-1}$, we obtain

$$\frac{1}{n}\partial_t(\partial_i\theta)^n + \frac{1}{n}(\boldsymbol{u} \cdot \nabla)(\partial_i\theta)^n + (\partial_i\theta)^{n-1}(\partial_i\boldsymbol{u} \cdot \nabla)\theta = \kappa(\partial_i\theta)^{n-1}\nabla^2\partial_i\theta + (\partial_i\theta)^{n-1}(\partial_i\boldsymbol{u}) \cdot \boldsymbol{G}. \tag{2.4}$$

The relevant physics in the bulk of the flow is associated with small volumes V with periodic boundaries. Taking the local volume average $\langle\cdot\rangle_V$, we obtain (no sum over i)

$$\frac{1}{n}\partial_t\langle(\partial_i\theta)^n\rangle_V + \langle(\partial_i\theta)^{n-1}(\partial_i\boldsymbol{u} \cdot \nabla)\theta\rangle_V = -\kappa\langle\nabla[(\partial_i\theta)^{n-1}] \cdot \nabla(\partial_i\theta)\rangle_V + \langle(\partial_i\theta)^{n-1}(\partial_i\boldsymbol{u}) \cdot \boldsymbol{G}\rangle_V. \tag{2.5}$$

The advective term disappears because of the boundaries chosen and the dissipative term is transformed by means of Green's formula.

The velocity field in the viscous–convective range is smooth and determined by its rate-of-strain tensor, $u_i(\boldsymbol{x}, t) = \sigma_{ij}(t)x_j$. Following Batchelor, we substitute the tensor by its principal components, denoted by σ_x, σ_y and σ_z. Incompressibility requires that

$\sigma_x + \sigma_y + \sigma_z = 0$, and we can take, without loss of generality, $\sigma_x > \sigma_y > \sigma_z$, i.e. $\sigma_x > 0$ and $\sigma_z < 0$. The principal axes will be randomly oriented in three-dimensional space, and their orientation will slowly vary in comparison with τ_η. This orientation is linked to the small-scale behaviour of the advecting turbulent flow which, we may assume, has no preferred direction (because the flow is assumed to be locally isotropic).

We should now specify the time dependence of the strain-rate tensor. Batchelor argued, on the basis of experiments by Townsend (1951), that $|\sigma_z|^{-1} \approx 2\tau_\eta$. We adopt the assumption that all three principal components vary on time scales larger than τ_η, and treat them as time-independent constants. From this consideration, the geometric coordinate system is rotated to coincide with the principal axes of the rate-of-strain tensor; for simplicity, the same notation as in the original coordinates is maintained hereafter. The velocity field becomes $\boldsymbol{u}(\boldsymbol{x}) = \sigma_x x \boldsymbol{e}_x + \sigma_y y \boldsymbol{e}_y + \sigma_z z \boldsymbol{e}_z$ and the mean scalar gradient vector, $\boldsymbol{G}$, that was originally pointing along one axis, now has three constant components in the new coordinates. Additionally, statistical stationarity is assumed. The statistical ensemble average, denoted by $\langle\cdot\rangle$, is taken as the average over volume and time. From (2.5), it follows (with $\sigma_i \neq 0$ and no sum over i) that

$$\langle(\partial_i\theta)^n\rangle \sim -\frac{\kappa}{\sigma_i}\langle\nabla[(\partial_i\theta)^{n-1}]\cdot\nabla(\partial_i\theta)\rangle + G_i\langle(\partial_i\theta)^{n-1}\rangle. \tag{2.6}$$

The resulting approximate balance is local and the volume under consideration should not be too large ($\sim\eta$). The physical idea, similar to that used in the inertial range of turbulence, is that a steady scalar intensity, sustained at scales larger than η, sweeps from these larger scales down to the viscous–convective range (the 'Batchelor cascade').

Equation (2.6) allows a further simplification. Successive insertion of (2.6) for moments of order $j-1$ into those of order j and use of homogeneity yields

$$\langle(\partial_i\theta)^n\rangle \sim -\frac{\kappa}{\sigma_i}\sum_{j=1}^{n-1} G_i^{j-1}\langle\nabla[(\partial_i\theta)^{n-j}]\cdot\nabla(\partial_i\theta)\rangle. \tag{2.7}$$

Consider now the direction of compression, i.e. the direction of the Batchelor cascade corresponding to $\sigma_z < 0$. For simplicity, we write $|\sigma_z| = \sigma$ and obtain for second order

$$\frac{\langle(\partial_z\theta)^2\rangle}{\kappa\langle[\nabla(\partial_z\theta)]^2\rangle} \sim \frac{1}{\sigma} = \text{constant}. \tag{2.8}$$

This can be checked by means of DNS. While the results were derived for the direction of compression in the coordinate system that is aligned with the principal axes, the DNS data analysis is done for the three original (outer) coordinates. However, the three outer coordinates combine linearly to the new z-coordinate. Thus, if we can examine the relation (2.8) for all three coordinates, we might obtain an adequate sense of its qualitative correctness. The comparisons are shown in figure 2. Both the numerator and denominator grow with increasing Sc. The inset in figure 2(b) plots their ratio for all three original coordinates. It can be seen that it is nearly constant, suggesting that the result (2.8) is plausible. This exercise also suggests that the denominator, which is the scalar gradient dissipation term, is directly related to the growth of the second-order derivative moment.

Similarly, the third-order moment follows the relation

$$\langle(\partial_z\theta)^3\rangle \sim (\kappa/\sigma)[\langle\nabla[(\partial_z\theta)^2]\cdot\nabla(\partial_z\theta)\rangle + G_z\langle[\nabla(\partial_z\theta)]^2\rangle], \tag{2.9}$$

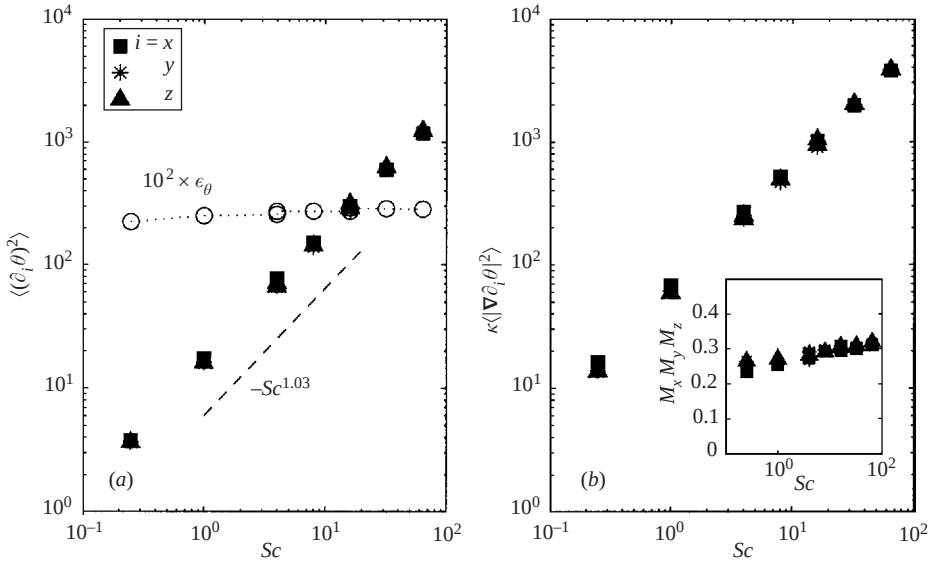

FIGURE 2. (*a*) Scalar derivative moments of second order, $\langle(\partial_i\theta)^2\rangle$, plotted against the Schmidt number, *Sc*. For comparison, we also plot the scalar dissipation rate, ϵ_θ (open circles) which is nearly constant. The dashed line indicates the power law that can be fitted to the data. (*b*) The scalar gradient dissipation rate, $\kappa\langle|\nabla\partial_i\theta|^2\rangle$, is plotted as a function of *Sc*. The inset shows the ratio (2.8), here denoted by M_x, M_y, and M_z, for the three coordinate directions. The mean scalar gradient is in the direction x. Symbols are indicated in the legends.

leading to the following expression for the skewness:

$$S_3(\partial_z\theta) = \frac{\langle(\partial_z\theta)^3\rangle}{\langle(\partial_z\theta)^2\rangle^{3/2}} \approx \sqrt{\frac{\sigma}{\kappa}}\left[\frac{\langle\nabla[(\partial_z\theta)^2]\cdot\nabla(\partial_z\theta)\rangle}{\langle[\nabla(\partial_z\theta)]^2\rangle^{3/2}} + \frac{G_z}{\langle[\nabla(\partial_z\theta)]^2\rangle^{1/2}}\right]. \tag{2.10}$$

Further progress is difficult without numerical back-up, but the above relation is of interest for an independent reason: the question can be raised if, for any finite value of κ and G, a relic of the large scale remains in the odd moments of the scalar derivative. The last term does not vanish within our approach although we should note that the first term remains 'uncontrolled' and cancellations might arise.

3. Upper bounds for unnormalized derivative moments

Equation (2.2) can be solved analytically using an ansatz in which the wave vector is a function of time, $\Theta(\boldsymbol{x}, t) = \Theta(t)\sin(\boldsymbol{k}(t)\cdot\boldsymbol{x})$. Here, the equation for the total passive scalar field is solved, this being a homogeneous problem in $\Theta(\boldsymbol{x}, t)$. Physically, we study the deformation of a cubic scalar blob or filament of initial side lengths $l_i = 2\pi/k_{i0}$ for $i = x, y, z$. Following Batchelor (1959), we take the initial condition to be $\Theta(\boldsymbol{x}, 0) = \Theta_0\sin(\boldsymbol{k}_0\cdot\boldsymbol{x})$.

Before continuing further, we express all quantities in their characteristic units, $\boldsymbol{k} = k_\eta\tilde{\boldsymbol{k}}$, $t = \tilde{t}\tau_\eta$, $\sigma = \tilde{\sigma}/\tau_\eta$, $\theta = \theta_{rms}\tilde{\theta}$ and $\kappa = \nu/Sc$. We define $k_\eta = \eta^{-1}$ and $\theta_{rms} = \langle\theta^2\rangle^{1/2}$. For simplicity, we set $\Theta_0/\theta_{rms} = 1$. The Batchelor wavenumber k_B becomes $\sqrt{Sc}$. The tilde for the dimensionless quantities is omitted in the following.

For $\boldsymbol{k} = (k_x, k_y, k_z)$ and coordinates $\boldsymbol{x} = (x, y, z)$ in the directions of the principal components of the rate-of-strain tensor, one arrives at the Batchelor solution for the

total scalar field

$$\Theta(\boldsymbol{x},t)=\exp\left[\frac{1}{2\sigma_x Sc}\left(k_x^2(t)-k_{x0}^2\right)+\frac{1}{2\sigma_y Sc}\left(k_y^2(t)-k_{y0}^2\right)+\frac{1}{2\sigma_z Sc}\left(k_z^2(t)-k_{z0}^2\right)\right]\times\sin(\boldsymbol{k}(t)\cdot\boldsymbol{x}),\quad(3.1)$$

with time-dependent wave-vector components

$$k_x(t)=k_{x0}\mathrm{e}^{-\sigma_x t},\qquad k_y(t)=k_{y0}\mathrm{e}^{-\sigma_y t},\qquad k_z(t)=k_{z0}\mathrm{e}^{-\sigma_z t},\quad(3.2)$$

where $\sigma_x>\sigma_y>0$ and $\sigma_z<0$. Consequently, the z-direction will be the direction of compression, leading to growth of $k_z(t)$ while $k_x(t)$ and $k_y(t)$ decrease exponentially with time. We now apply Batchelor's solution to the derivative moments. With (2.1), a binomial expansion for the nth power of the partial derivative of the turbulent scalar fluctuations in the ith direction gives

$$(\partial_i\theta)^n=(\partial_i\Theta+G_i)^n=\sum_{m=0}^{n}\frac{n!}{m!\,(n-m)!}\,(\partial_i\Theta)^m\,G_i^{n-m}.\quad(3.3)$$

For times $t\sim\tau_\eta$ the exponential term with respect to the direction of compression, z in our case, becomes dominant. We can neglect the contribution arising from $k_x(t)$ and $k_y(t)$ and obtain, by combining (3.1) and (3.3), the relation

$$(\partial_i\theta)^n\approx\sum_{m=0}^{n}\frac{n!}{m!\,(n-m)!}\,k_i^m(t)\exp\left(-\frac{mk_{z0}^2\mathrm{e}^{2\sigma t}}{2\sigma\,Sc}\right)\cos^m(\boldsymbol{k}(t)\cdot\boldsymbol{x})G_i^{n-m},\quad(3.4)$$

where, again, $\sigma=|\sigma_z|$ has been used.

Time averaging is inappropriate here because the gradient solution (3.4) is exponentially increasing in time in the direction of compression. Nevertheless, statistical averages can be performed in two different ways. The first, suggested by Kraichnan (1968), is to integrate over a probability density function that characterizes the distribution of the principal strain rates. We suggest an alternative in which the averaging can be performed over an ensemble of initial wave vectors $\boldsymbol{k}_0$ in the viscous–convective range, characterizing the shape and extent of scalar filaments. The filaments are expected to possess wavenumbers up to k_B. One then has

$$\langle(\partial_i\theta)^n\rangle_{\boldsymbol{k}_0}=\int\mathrm{d}^3k_0\,(\partial_i\theta)^n\,p(\boldsymbol{k}_0),\quad(3.5)$$

where $p(\boldsymbol{k}_0)$ is the probability density of the initial wavevectors $\boldsymbol{k}_0$. The simplest case for $p(\boldsymbol{k}_0)$ is to assume that all wave vectors $\boldsymbol{k}_0$ (positive as well as negative ones!), whose absolute values lie within the viscous–convective range, are equally likely. In dimensionless and normalized form, this distribution assumes an equipartition shape over the viscous–convective range, and is given by $p(\boldsymbol{k}_0)=1/[8(\sqrt{Sc}-1)^3]\prod_{i=1}^{3}\mathrm{H}(\sqrt{Sc}-k_{0i})\,\mathrm{H}(k_{0i}-1)$ where $\mathrm{H}(x)$ is the Heaviside function, which is 1 for $x>0$ and 0 for $x<0$. We define $\Omega\equiv[-\sqrt{Sc},-1]^3\times[1,\sqrt{Sc}]^3$ as the subspace of wave vectors in the viscous–convective range. For the nth moment of the scalar derivative, we then have to solve

$$\langle(\partial_i\theta)^n\rangle_{\boldsymbol{k}_0}=\sum_{m=0}^{n}\frac{n!}{m!\,(n-m)!}\,\frac{G_i^{n-m}}{8(\sqrt{Sc}-1)^3}\int_\Omega\mathrm{d}^3k_0\,(\partial_i\Theta)^m,\quad(3.6)$$

which results from combining (3.4) and (3.5) with $p(\boldsymbol{k}_0)$. The mean gradient appears in different powers in the sum. For any non-vanishing mean gradient, the upper

bound consists of a constant and Sc-independent part. The average is also still a function of time and local space coordinates. We are interested in maximum values of the derivative moments, i.e. upper bounds of the integral expression (3.6). The Batchelor solution still contains the oscillating spatial cosine contribution coming from the initial ansatz. Performing additionally an average over the blob volume in (3.5) would lead to zero values for all orders. This is a shortcoming of the simple shape of the scalar filament. We can use the boundedness of the oscillating part, i.e. $\cos^m(\boldsymbol{k}\cdot\boldsymbol{x}) \leqslant 1$, to calculate upper bounds of the scalar derivative moments within the blob, using Batchelor's quasi-static straining approximation. In detail, we have

$$\begin{aligned}\langle(\partial_i\theta)^n\rangle_{\boldsymbol{k}_0} &= \sum_{m=0}^{n} \frac{n!}{m!\,(n-m)!} G_i^{n-m} \mathrm{e}^{-m\sigma_i t} \\ &\quad\times \frac{1}{8(\sqrt{Sc}-1)^3} \int_{\Omega} \mathrm{d}^3k_0\; k_{i0}^m \exp\left(-\frac{mk_{z0}^2\mathrm{e}^{2\sigma t}}{2\sigma\, Sc}\right) \cos^m(\boldsymbol{k}(t)\cdot\boldsymbol{x}) \\ &\leqslant \sum_{m=0}^{n} \frac{n!}{m!\,(n-m)!} |G_i|^{n-m} \mathrm{e}^{-m\sigma_i t} \\ &\quad\times \frac{1}{(\sqrt{Sc}-1)^3} \int_{1}^{\sqrt{Sc}} \mathrm{d}^3k_0\; |k_{i0}|^m \exp\left(-\frac{mk_{z0}^2\mathrm{e}^{2\sigma t}}{2\sigma\, Sc}\right) \equiv \overline{\langle(\partial_i\theta)^n\rangle}_{\boldsymbol{k}_0}. \end{aligned} \tag{3.7}$$

We note that for $t = \sigma^{-1}\ln(k_\eta\sqrt{Sc}/k_{z0})$ the wavenumber exceeds the Batchelor value and spreads into the viscous–diffusive range, where it is damped. This can be seen by inserting $k_B = \sqrt{Sc}\,k_\eta$ into (3.2). This is roughly the time at which the present picture becomes internally inconsistent. We also note that, because the bounds for unnormalized moments have been taken already, we cannot use this result to obtain bounds for normalized moments.

We should distinguish between two cases: the evolution of the derivative moments in the directions of compression (z with $\sigma_z < 0$) and expansion (at least x with $\sigma_x > 0$; the y direction is neutral when $\sigma_y = 0$). For the expansion, we obtain a rapid decrease of the upper bounds. The filament is expanding exponentially in directions of positive strain rate, thus reducing the scalar gradients rapidly. The interesting case occurs in the direction of compression, which we now discuss. The relevant equation is

$$\overline{\langle(\partial_z\theta)^n\rangle}_{\boldsymbol{k}_0} = \sum_{m=0}^{n} \frac{n!}{m!\,(n-m)!} |G_z|^{n-m}\mathrm{e}^{m\sigma t} \frac{1}{\sqrt{Sc}-1} \int_{1}^{\sqrt{Sc}} \mathrm{d}k_{z0}\; k_{z0}^m \exp\left(-\frac{mk_{z0}^2\mathrm{e}^{2\sigma t}}{2\sigma\, Sc}\right). \tag{3.8}$$

The integral in (3.8) can be written as

$$I_m = \frac{1}{2}\left(\frac{\mathrm{e}^{2\sigma t}m}{2\sigma\, Sc}\right)^{-(m+1)/2} \left[\Gamma\left(\frac{m+1}{2}, \frac{\mathrm{e}^{2\sigma t}m}{2\sigma\, Sc}\right) - \Gamma\left(\frac{m+1}{2}, \frac{\mathrm{e}^{2\sigma t}m}{2\sigma}\right)\right], \tag{3.9}$$

where $\Gamma(z,a) = \int_a^\infty \mathrm{e}^{-t}\, t^{z-1}\,\mathrm{d}t$ is the incomplete Gamma function with $\Gamma(z,0) = \Gamma(z)$ (Abramowitz & Stegun 1972).

Clearly, the bound depends on both Sc and the magnitude of G. It also remains time-dependent as does the Batchelor solution for the passive scalar field itself. Again, the physical picture is that scalar substance sweeps steadily from scales larger than η into the viscous–convective range where it is advected down to scales of the order η_B, and dissipated diffusively beyond. For this reason, it can be suggested that the average over the initial wavenumbers is equivalent to a common time average taken

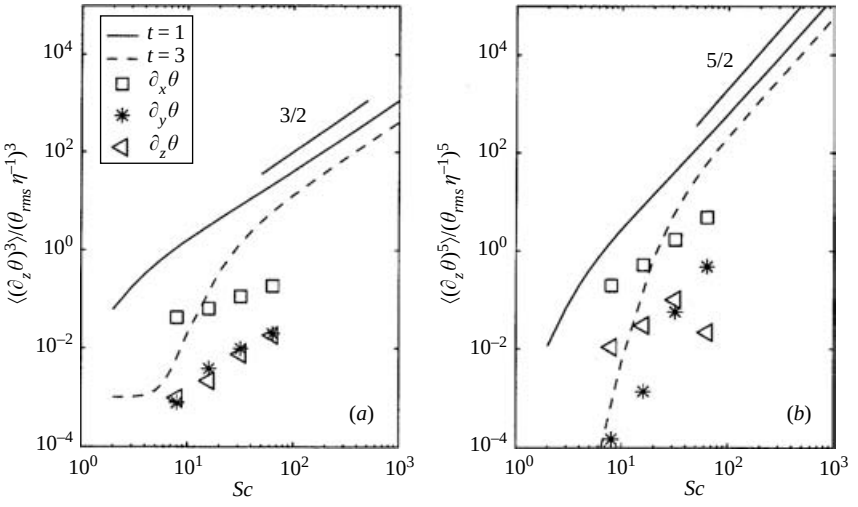

FIGURE 3. Comparison of the upper bounds for the moments $\langle(\partial_z\theta)^n\rangle(\theta_{rms}\eta^{-1})^n$ with DNS results at $R_\lambda = 38$ and $Sc = 8, 16, 32$ and 64: (*a*) the third order, and (*b*) the fifth. Solid lines are for $t/\tau_\eta = 1$, dashed lines are for $t/\tau_\eta = 3$. $\sigma\tau_\eta$ was taken to be $1/2$. Slopes of $3/2$ and $5/2$ are also indicated by straight lines. The mean gradient is $G/(\theta_{\rm rms}\eta^{-1}) = 0.10$. The DNS data correspond to normalized $G/(\theta_{rms}\eta^{-1})$ values between 0.02 and 0.05.

in DNS, namely by assuming a kind of ergodicity. The bound will be determined by the leading term in the sum in (3.8), and is given, for the case $Sc \to \infty$, always by

$$\overline{\langle(\partial_z\theta)^n\rangle}_{\mathbf{k}_0} \sim Sc^{n/2}. \tag{3.10}$$

This conclusion is meaningful only if $Sc \gg 1$ and a developed viscous–convective scaling range exists. For intermediate Sc or for strong gradient forcing we can expect crossovers in the dominance of one of the $n+1$ terms (see equation (3.3)).

In order to compare the upper bound results with DNS, we evaluated the bound (3.8) as well as the derivative moments numerically. Figure 3 shows the result for two different times t. We observe that the upper bound slowly decreases with time, but is roughly consistent with the DNS results. In general, the DNS results, indicated by the symbols, are smaller than the bound. Because the coordinate system used here is rotated into the principal axes, and not the one used in the DNS, derivative moments from the latter are plotted for all three directions. It can be expected that their linear combination also does not exceed the bound. We see that their growth with Sc is different from the upper bound. While the x-derivative grows with exponents of ≈ 0.75 and ≈ 1.4 for the third and the fifth moments, respectively, the y- and z-derivatives follow a $3/2$ power for order 3, and show no scaling for order 5.

The G-dependence of the bounds is presented in figure 4 for four values of G. Clearly, the bounds level off at larger magnitudes for increasing G in the limit of $Sc \to 1$. This is followed by a crossover region which ends in an algebraic scaling of the nth-order moment according to the power $n/2$. This is due to the first term in the sum (3.8). For intermediate Sc, the upper bound behaves as in the DNS data.

4. Conclusions

We have investigated the large-Sc behaviour of derivative moments in scalar turbulence sustained by a mean scalar gradient. The smooth velocity field advecting

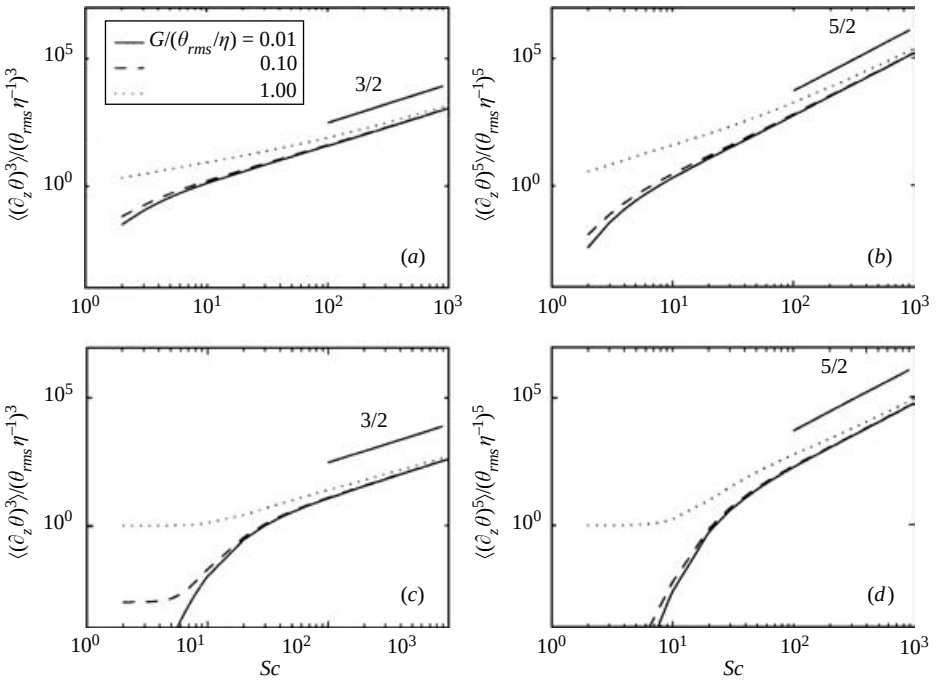

FIGURE 4. Dependence of the upper bounds of the moments $\langle(\partial_z\theta)^n\rangle(\theta_{rms}\eta^{-1})^n$ on the mean scalar gradient G for $n = 3$ and 5: (a, b) $t = 1$, (c, d) $t = 3$. Values of G are measured in units of θ_{rms}/η, as indicated in the legends.

the scalar in the viscous–convective range is assumed to possess quasi-static principal rates of strain, as in Batchelor's (1959) model. A relation for the nth-order derivative moment in terms of the mean gradient, G, and the scalar gradient dissipation is derived. The result agrees well with DNS results for the second order (see inset to figure 2*b*). Batchelor's model of quasi-static principal rates of strain is used to calculate upper bounds for scalar derivative moments. The bounds are consistent with numerical findings for $Sc \gg 1$. The mean scalar gradient forcing included in the model results in crossover regimes for intermediate Sc, depending on their relative magnitudes. In this range, the growth of the bounds approaches the numerical findings.

Unfortunately, there are a few aspects of the problem that cannot be captured in the approach. As can be seen in figure 1 there are qualitative differences between even- and odd-order normalized moments which should cause similar differences in unnormalized moments. In this connection, we can combine the numerical result of figure 2, that the second-order moment grows as $Sc^{1.03}$, with equation (3.10), which shows that the third-order moment grows as $Sc^{1.5}$, and conclude that the skewness decays slowly as $Sc^{-0.045}$, but this is slow compared to the numerical data of figure 1. Secondly, the single Fourier mode ansatz for the initial filament is simplistic and unsuitable for discussing the ramp–cliff structure. Whether the present quasi-static approach or Kraichnan's alternative is closer to the physics in the viscous–convective scaling range can only be answered by means of more detailed numerical investigations.

We thank A. Bershadskii, J. Davoudi and B. Eckhardt for fruitful discussions, and Shuyi Xu for her help in making the DNS data available. For financial

support, J. S. thanks the Feodor-Lynen Fellowship Program of the Alexander-von-Humboldt Foundation, and K. R. S. and P. K. Y. acknowledge the US National Science Foundation. Computer time was provided by the San Diego Supercomputer Center within the NPACI program.

REFERENCES

Abramowitz, M. & Stegun, I. A. 1972 *Handbook of Mathematical Functions*. Dover.

Antonia, R. A. & Orlandi, P. 2002 Dependence of the second-order scalar structure function on the Schmidt number. *Phys. Fluids* **14**, 1552–1554.

Balkovsky, E. & Fouxon, A. 1999 Universal long-time properties of Lagrangian statistics in the Batchelor regime and their application to the passive scalar problem. *Phys. Rev.* E **60**, 4164–4174.

Batchelor, G. K. 1959 Small scale variation of convected quantities like temperature in a turbulent fluid. *J. Fluid Mech.* **5**, 113–133.

Bogucki, D., Domaradzki, J. A. & Yeung, P. K. 1997 Direct numerical simulations of passive scalars with $Pr > 1$ advected by turbulent flow. *J. Fluid Mech.* **343**, 111–130.

Brethouwer, G., Hunt, J. C. R. & Nieuwstadt, F. T. M. 2003 Micro-structure and Lagrangian statistics of the scalar field with a mean gradient in isotropic turbulence. *J. Fluid Mech.* **474**, 193–225.

Celani, A., Lanotte, A., Mazzino, A. & Vergassola, M. 2001 Fronts in passive scalar turbulence. *Phys. Fluids* **13**, 1768–1783.

Corrsin, S. 1951 On the spectrum of isotropic temperature fluctuations in isotropic turbulence. *J. Appl. Phys.* **22**, 469–473.

Dahm, W. J. A., Southerland, K. B. & Buch, K. A. 1991 Direct, high resolution, four-dimensional measurements of the fine scale structure of $Sc \gg 1$ molecular mixing in turbulent flows. *Phys. Fluids* **A3**, 1115–1127.

E, W. & Vanden-Eijnden, E. 2001 Turbulent Prandtl number effect on passive scalar advection. *Physica* D **152–153**, 636–645.

Gibson, C. H., Friehe, C. A. & McConnell, S. O. 1977 Skewness of temperature derivatives in turbulent shear flows. *Phys. Fluids Suppl.* **20**, 156–167.

Holzer, M. & Siggia, E. D. 1994 Turbulent mixing of a passive scalar. *Phys. Fluids* **6**, 1820–1837.

Kraichnan, R. H. 1968 Small-scale structure of a scalar field convected by turbulence. *Phys. Fluids* **11**, 945–953.

Obukhov, A. M. 1949 Structure of the temperature field in turbulent flows. *Isv. Geogr. Geophys.* **13**, 58–69.

Prasad, R. R. & Sreenivasan, K. R. 1990 Quantitative three-dimensional imaging and the structure of passive scalar fields in fully turbulent flows. *J. Fluid Mech.* **216**, 1–34.

Pumir, A. 1994 A numerical study of the mixing of a passive scalar in three dimensions in the presence of a mean gradient. *Phys. Fluids* **6**, 2118–2132.

Saylor, J. R. & Sreenivasan, K. R. 1998 Differential diffusion in low Reynolds number water jets. *Phys. Fluids* **10**, 1135–1146.

Sreenivasan, K. R., Antonia, R. A. & Britz, D. 1979 Local isotropy and large structures in a heated turbulent jet. *J. Fluid Mech.* **94**, 745–775.

Sreenivasan, K. R. & Antonia, R. A. 1997 The phenomenology of small-scale turbulence. *Annu. Rev. Fluid Mech.* **29**, 435–472.

Townsend, A. A. 1951 On the fine-scale structure of turbulence. *Proc. R. Soc. Lond.* A **208**, 534–542.

Yaglom, A. M. 1949 O lokalnoi strukture polya temperatur v turbulentnom potoke. *Dokl. Akad. Nauk SSSR* **69**, 743–746.

Yeung, P. K., Xu, S. & Sreenivasan, K. R. 2002 Schmidt number effects on turbulent transport with uniform mean scalar gradient. *Phys. Fluids* **14**, 4178–4191.